Accepted Manuscript

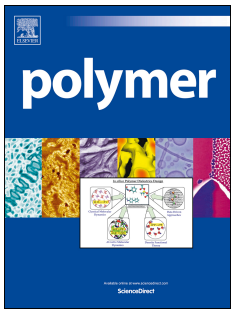

Enthalpy recovery of ultrathin polystyrene film using Flash DSC

Yung P. Koh, Sindee L. Simon

PII: S0032-3861(18)30163-0

DOI: 10.1016/j.polymer.2018.02.038

Reference: JPOL 20386

To appear in: *Polymer*

Received Date: 18 December 2017

Revised Date: 10 February 2018

Accepted Date: 17 February 2018

Please cite this article as: Koh YP, Simon SL, Enthalpy recovery of ultrathin polystyrene film using Flash DSC, *Polymer* (2018), doi: 10.1016/j.polymer.2018.02.038.

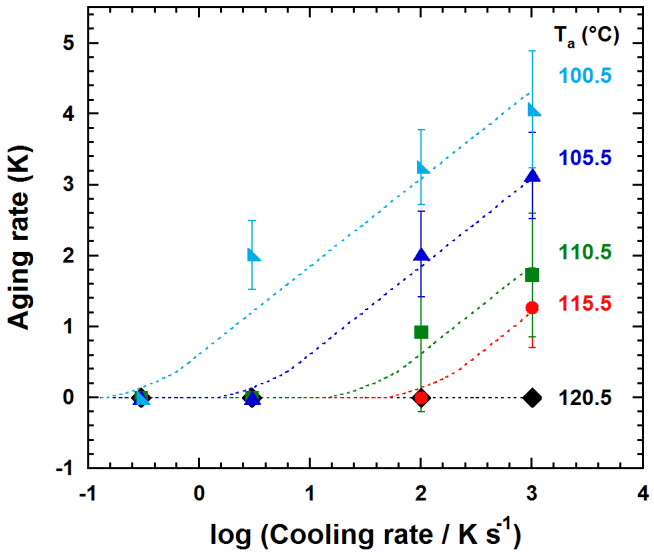

Enthalpy Recovery of Ultrathin Polystyrene Film Using Flash DSC

Yung P. Koh and Sindee L. Simon

Department of Chemical Engineering, Texas Tech University, Lubbock, TX 79409-3121, USA

Enthalpy recovery for a single polystyrene ultrathin film of 20 nm thickness is studied using Flash DSC over an extended time and temperature range. Results are compared to a bulk sample of the same polystyrene using a similar experimental protocol and analysis procedure in an effort to determine the effects of nanoconfinement. Examined is the cooling rate dependence of the glass transition temperature (T_g) of unaged films which informs the initial fictive temperature (T_{fo}) and thus the jump size (T_{fo} - T_a) for a given aging temperature (T_a). Isothermal enthalpy recovery is investigated as a function of both T_a for various cooling rates and as a function of jump size at constant T_a. The apparent activation energies at T_g and along the glassy line are determined and compared, as is the enthalpy recovery aging rate. Although the apparent activation energy along the glass line is the same within experimental error as the bulk, the aging rate is found to be slightly faster in the ultrathin film. Increasing the cooling rate prior to aging increases the aging rate. The results are discussed in the context of the two competing factors which influence the aging rate, namely, the driving force and the molecular mobility. The driving force for aging is dictated by the jump size or cooling rate, i.e., the value of T_{fo} - T_a. The mobility, on the other hand, is dictated by the relaxation time at the aging temperature, which increases during aging from the value on the initial glass line to that at equilibrium. The initial mobility in the glassy state is dictated by the jump size, being related to T_{fo} - T_a and the temperature dependence of the relaxation time along the glass line, whereas the mobility at equilibrium is dictated by T_a, T_g, and the temperature dependence and breadth of the equilibrium relaxation time.

Introduction

Structural recovery occurs in the glassy state due to the non-equilibrium nature of glasses. During structural recovery, thermodynamic and mechanical properties spontaneously evolve towards their corresponding equilibrium values. Such changes in properties may directly affect the reliability and integrity of glasses in practical applications and are important for the long-term stability of glasses.[1-6]

Nanoconfinement has been found to affect structural recovery [7-15], but rates are reported to be enhanced [16,17], retarded [10,11], or unchanged [8,9] relative to the bulk, depending on the material, type of confinement, and measurement technique. In previous work [14,18-20] using Flash DSC (differential scanning calorimetry), we exploited the fast response time and high scanning rate to study the enthalpy recovery of high fictive temperature glasses at short aging times and high aging temperatures, thereby significant reducing the timescale of these generally labor-intensive experiments by more than two orders of magnitude. In this work, the glass transition and enthalpy recovery behavior measured by Flash DSC of an ultrathin film and a thicker "bulk-like" film are further compared, particularly the competing effects of jump size and aging temperature on the aging rate. Results discussed also include the cooling rate dependence of T_g, apparent activation energy at T_g and along the glassy line, and the evolution of the fictive temperature (T_f) as a function of aging temperature (T_a).

Methodology

Polystyrene of 1,998,000 g/mol and PDI of 1.02 (Sigma-Aldrich) is used, as in our previous works.[14,18-21] Film and sample preparation methods have been reported,[14,18,19] and important protocols are repeated here for the sake of completeness. Two sample film thicknesses

are compared, those of 20 nm and 1.1 μm for ultrathin and thin films, respectively, as measured by atomic force microscope in tapping mode. Flash DSC sample masses were estimated to be approximately 5.0 ng for the 20 nm thick ultrathin film and 81 ng for 1.1 μm thick thin film based on the sample dimensions, density, and step change in heat capacity at T_g (ΔC_p).

The commercially available fast scanning calorimetry, Mettler Toldeo Flash DSC, was employed both for isothermal enthalpy recovery (aging) experiments and T_f measurements on heating after aging, as well as after cooling at different rates ranging from 0.1 to 1000 K/s. For all thermal histories, the sample was first held at 190 °C for 6 s to erase any prior thermal history. After a given thermal history, T_f was then measured on heating at 600 K/s. For isothermal enthalpy recovery, samples were cooled at 1000 K/s to various aging temperatures ranging from 50.5 to 120.5 °C and aged for times ranging from 0.01 to 60000 s. After aging, samples were cooled to 30 K and then the heating scan was performed. Limited aging experiments at high aging temperatures were also performed after cooling at rates of 0.3, 3, and 100 K/s.

Enthalpy recovery was monitored by following the fictive temperature T_f. As introduced by Tool [22], T_f is defined as the intersection of the extrapolated glass line and the extrapolated liquid line and is a measure of the structure of the glassy state or the departure from equilibrium. During structural recovery T_f evolves from an initial fictive temperature (T_{fo} or T_f') to a long-time limiting value ($T_{f\infty}$) equal to the aging temperature (T_a) assuming that the extrapolated liquid line is reached at equilibrium. The fictive temperature is calculated from Flash DSC heating scans by integrating the heat capacity using the area matching Moynihan's method [23] or a simplified version [21] for the case when T_f is below the onset of devitrification , as mathematically defined in equations (1) and (2), respectively:

$$\int_{T_f}^{T>>T_g}(C_{pl}-C_{pg})dT=\int_{T<<T_g}^{T>>T_g}(C_p-C_{pg})dT \quad (1)$$

$$\int_{T_f}^{T>>T_g}(C_{pl}-C_p)dT=0 \quad (2)$$

where C_{pl} is the liquid heat capacity, C_{pg} is the glass heat capacity, and C_p is the heat capacity of sample. Compared to the original Moynihan's method (equation (1)), the simplified version (equation (2)) requires only the extrapolated liquid line and, thus, results in a more accurate T_f calculation when T_f is below the onset of the enthalpy recovery peak [21]. Since, the T_f calculation strongly depends on an unbiased liquid line (and glass line in the case of the original Moynihan's method), care was taken to ensure accurate lines are drawn by obtaining these from the average of ten unaged scans. Then, each heating scan was superposed with this averaged unaged scan by minimizing χ^2 method for regions away from the enthalpy overshoot and transition.[14,18-21].

The Flash DSC chip sensors were preconditioned and calibrated before the sample loading following the manufacturer recommendation without further additional correction. In our previous work [14], this manufacturer calibration is found to be valid within 0.6 ± 0.7 K. The calibration of isothermal temperatures for aging temperatures follows our prior Flash DSC work such that the actual isothermal temperature is 0.5 K higher than the program temperature.

Results

The comparison of Flash DSC scans for 20 nm thick ultrathin and 1.1 μm thick thin films are shown in Figure 1, as a function of cooling rate from 0.1 K/s to 1000 K/s. The magnitude of

heat flow is directly proportional to the sample mass, which differs by approximately 17 times between 20 nm and 1.1 μm films, as reflected by the two scale bars. With decreasing cooling rate, for both samples, the enthalpy overshoot shifts to higher temperature and its magnitude increases, leading to a lower value of T_f as cooling rate decreases. The enthalpy overshoot of the ultrathin film is broader than the 'bulk-like' sample and this broadening is enhanced as cooling rate decreases, resulting in a T_g depression. Although the enthalpy overshoot peaks shown in Figure 1 are at the similar position (temperature) for both bulk and ultrathin film, devitrification begins much earlier (at lower temperature) for ultrathin film and the overshoot area is larger.

Based on Flash DSC scans of Figure 1, the limiting fictive temperature T_f' which is found to be equivalent to T_g for a given cooling and heating rate [23], is calculated and the resulting T_f' as a function of the logarithm of the cooling rate q is plotted in Figure 2a for the 20 nm thick film and "bulk" data. The T_f' of the 20 nm thick film is similar within experimental error to that of the bulk at high cooling rates, but significantly depressed from the bulk at slower cooling rates, with a 12 K depression at a cooling rate of 0.1 K/s. The magnitude of the depression at the slowest rate is consistent with the results in the literature [24-26]. The dependence of the T_g depression on cooling rate is also consistent with our prior works [8,18,21] and the literature [27,28] and can be described by the Williams-Landell-Ferry (WLF) [29] expression. The apparent normalized activation energy ($E_a/R = \partial \ln q / \partial 1/T_f'$) is 71 ± 3 and 105 ± 3 kK for the 20 nm thick film and the bulk, respectively, at the nominal T_g (measured at 0.1 K/s) and the corresponding fragility (m) values are 85 ± 4 and 122 ± 4. The same data can be used to obtain the average relaxation time at T_g, as shown in Figure 2b, based on the relationship between the cooling rate and relaxation time from Hodge ($\tau = RT_g^2/qE_a$) [5], which can be derived from an effective time assumption. It should be noted that the relaxation time is not simply the inverse of the cooling

rate, and making such an assumption results in an underestimation of τ by nearly 30% for the bulk film and twice that for the 20 nm-thick ultrathin film.

Representative Flash DSC scans are compared in Figure 3 as a function of aging time for 20 nm and 1.1 μm thick films after cooling at 1000 K/s and aging isothermally at 100.5 °C. With increasing aging time, the enthalpy overshoots grow in magnitude and shift to higher temperatures, similar to the effect of decreasing cooling rate in Figure 1. The developing enthalpy overshoots in both Figures 1 and 3 are due to a continuously decreasing mobility associated with the decrease in enthalpy and volume which occurs due to relaxation during cooling for Figure 1 and due to relaxation during isothermal aging for Figure 3. For the longest aging times in Figure 3, the Flash DSC scans for a given sample superpose and the values of T_f level off at approximately T_a = 100.5 °C within experimental error, indicating that equilibrium is reached for both the 20 nm and the bulk sample. Compared to the bulk, the Flash DSC scans for the thin film show a broader transition on the low temperature side, with devitrification occurring earlier, again indicating the broader relaxation time distribution under nanoconfinement.

The progression of enthalpy recovery for the 20 nm ultrathin film at aging temperatures from 100.5 to 120.5 °C is shown in Figure 4a in terms of the evolution of T_f. The initial T_f (T_{fo} or T_f') is the same at 116.6 ± 2.5 °C for all experiments since it is dictated by the cooling rate, which was 1000 K/s for these experiments. T_f decreases during cooling and levels off at T_a for the three lowest aging temperatures of 100.5, 105.5, and 110.5 °C, resulting in $T_{f\infty} = T_a$ within experimental error. However, in case of T_a = 115.5 °C, $T_{f\infty}$ is lower than T_a at a value of 112.7 ± 0.6 °C due to relaxation during cooling through the transition region after isothermal aging and prior to the heating scan where T_f was measured. This behavior is consistent with that of the

bulk sample when T_a is in transition region and can be quantitatively modeled using the TNM/KAHR model of structural recovery assuming that the equilibrium liquid line where $T_f = T_a$ is reached during isothermal aging.[18] In addition, for T_a = 120.5 °C, T_f is unchanged from T_{fo} since the sample is in the equilibrium state, above the T_g region, at this aging temperature.

The evolution of T_f due to enthalpy recovery at lower aging temperatures ranging from 50.5 to 90.5 °C, is shown in Figure 4b. Contrary to the case of high T_a, here, aging is not complete in the time scale of the measurements (60,000 s) and T_f does not level off. The data in Figure 4b also show a distinct initial plateau where no aging occurs. The length or time scale of the plateau or inductive time (t_{ind}) increases as T_a decreases, similar to our previous results for bulk films [19], indicating that the molecular mobility along the glass line (at constant $T_f = T_f'$) decreases with decreasing temperature.

The temperature dependence of the relaxation time along the glass line and the corresponding apparent activation energy in the glassy state can be obtained by aging time-temperature superposition. The data of Figures 4a and b are reduced by aging time-temperature superposition, in which the T_f curves are shifted horizontally along the logarithmic aging time axis, taking 90.5 °C as a reference. The resulting reduced curves are shown in Figure 4c and are smooth and well superposed except after equilibrium is reached at the highest aging temperatures and T_f levels off to its equilibrium value. The apparent activation energy along the glass line is obtained from an Arrhenius plot of the logarithmic shift factor ($\ln a_T$) as shown in Figure 5, along with previous data for the bulk [19] for aging temperatures from 50.5 to 110.5 °C. The resulting apparent activation energy along the glass line is found to be 13.0 ± 1.2 kK from the slope of Figure 5, the same as that of the bulk (13.2 ± 0.6 kK) within experimental error, and consistent with our prior analysis of the temperature dependence of the induction time [14]. On the other

hand, the data for T_a = 115.5 °C, as represented by empty symbols, has a higher shift factor than expected, presumably due to the additional relaxation during cooling after aging at this temperature, as previously discussed.

In addition to the apparent activation energy along the glass line, the aging rate can be determined from the evolution of T_f. The aging rate can be quantified by the slope in the region where T_f decreases linearly with respect to logarithmic time [8]:

$$R = -\frac{dT_f}{d\log t_a} \qquad (3)$$

The units for the aging rate R are K per decade of the aging time and the minus sign is introduced to make the quantity positive. Aging rates are zero above T_g, increase as T_a decreases and then plateau off or slightly decrease with decreasing T_a, as shown in Figure 6. The aging rates of the 20 nm ultrathin film are comparable to the bulk film near T_g but slightly higher between 50 and 100 °C, with a maximum rate at approximately 80 °C.

The aging rate depends on the temperature jump size, the time required to obtain equilibrium (t_∞, or the longest relaxation time) and the induction time. To a first approximation, we can write

$$R \approx \frac{T_f' - T_a}{\log(t_\infty / t_{ind})} \qquad (4)$$

where the temperature jump size is the difference between the limiting fictive temperature T_f' (or the initial fictive temperature T_{fo}) and the aging temperature T_a. In reality, equation (4) underestimates the aging rate due to the curvature of the T_f vs log time response at short and long

times, before and after the region where T_f is approximately linear with logarithmic time. Nevertheless, when aging rates are compared between nanoconfinement and the bulk, any change in T_g (or T_f') under nanoconfinement should be taken account, such that the comparison is made at the same distance from T_g, not at the same aging temperature.[8] In this work, the T_g depression of the nanoconfined film is negligible for the cooling rate of 1000 K/s, and thus, the comparisons are made at the same temperature. In contrast to our result here where aging rates are higher for the thin film below 100°C, stacked ultrathin films [8] and nanospheres [9] showed the same aging rates as the bulk when compared the same distance from T_g, whereas supported ultrathin films showed lower aging rates [10,11]. Whether the difference is due to the high fictive temperature glass created in this work by cooling at 1000 K/s, which is approximately three orders of magnitude faster than the cooling rates used in the other works [8-11], is unclear.

For the results shown thus far, T_f' = 116.6 °C for a cooling rate of 1000 K/s. We can change the jump size at constant T_a by simply varying the cooling rate. For example, from Figure 2, T_f' is 106.7 ± 3.1, 96.7 ± 2.0, and 91.7 ± 3.2 °C for cooling rates of 100, 3, and 0.3 K/s. The evolution of T_f as a function of aging time for a cooling rate of 100 K/s and T_f' = 106.7 °C is shown in Figure 7a as a function of aging temperature. In this case, no aging is observed at T_a = 115.5 and 120.5 °C because the material is in the equilibrium state above the glass transition region and relatively far above the T_g (or T_f') value of 106.7 °C. At T_a = 110.5 °C, a small amount of aging is observed since T_a is in the vicinity of T_g (106.7 °C). In addition, the long-time value of T_f for the lowest three aging temperatures is below T_a due to the relaxation that occurs during cooling after aging. As cooling rate decreases to 3 K/s and T_f' = 96.7 °C, as shown in Figure 7b, aging is only observed at 100.5 °C since the material is in equilibrium at the higher

aging temperatures. Finally, for a cooling rate of 0.3 K/s and T_f' = 91.7 °C, shown in Figure 7c, no aging is observed for any of the aging temperatures investigated. Combining the results of Figures 7a – c with Figure 4a shows three limiting behaviors depending on the jump size: 1) $T_{f\infty} = T_a$ when T_a is far below T_f' (i.e., below the glass transition region), 2) $T_{f\infty} < T_a$ when T_a is close to T_f' (within the glass transition region), 3) $T_{f\infty} = T_f'$ when T_a is far above T_f' (above the glass transition region). Similar behavior was observed and modeled for the bulk [18]. Perhaps more importantly, these results also support the T_g depression in the ultrathin film because no aging is observed for the thin film at temperatures where aging is observed for the bulk: for example, for the bulk, aging is observed at 115.5 °C after 100 K/s cooling and at 105.5 °C after 3 K/s cooling, [18] whereas no aging is observed under nanoconfinement in these conditions. This result is unambiguous evidence of the depressed T_g in the nanoconfined sample.

Two competing factors determine the rate of structural recovery – the driving force and the molecular mobility. The driving force is proportional to the jump size and the mobility is dictated by the relaxation time at the aging temperature, which increases during aging from an initial value in the glassy state to the equilibrium long-time limit. In terms of equation (4), the jump size is the numerator, whereas the aging temperature influences the denominator primarily through the value of the time required to reach equilibrium t_∞, which depends on the equilibrium relaxation time and the breadth of relaxation time distribution (since t_∞ is larger than average at equilibrium [14]). Importantly the value of t_∞ is independent (or nearly independent) of jump size for down jumps [3,18,30] although it does depend on T_a, T_g, and the temperature dependence of the equilibrium relaxation time distribution (through, for example, the WLF equation [29]). On the other hand, t_{ind} depends on the aging temperature, jump size (T_{fo} - T_a) or cooling rate, and the value of E_a along the glassy line. The competing effects of jump size and

aging temperature can be clearly demonstrated by examining the rate of aging as a function of logarithmic cooling rate, as shown in Figure 8. As logarithmic cooling rate increases, the aging rate at a given T_a increases approximately linearly with a slope of nearly unity. As shown in the inset, the aging rate as a function of T_{fo} appears to have a similar linearity, due to the approximately linear relationship between T_{fo} (T_f') and log q over a small range of log q. On the other hand, at a constant cooling rate q, the aging rate increases as T_a decreases near T_g, with a maximum in rate reached, as shown in Figure 6, at approximately 80 °C for q = 1000 K/s. Due to this interplay between the driving force and mobility, care must be taken when comparing aging rates for samples having different T_g values or when comparing results in the literature where very different cooling rates were used.

Conclusions

The enthalpy recovery behaviors of a single 20 nm film and a 1.1 μm thick film are investigated using Flash DSC. The 20 nm ultrathin film has a broader glass transition region than the bulk, resulting in depressed T_g and a broader relaxation time distribution. The ultrathin film also shows a higher temperature dependence of T_g on cooling rate and a reduced apparent activation energy and fragility at T_g. Three types of limiting aging behavior depending both on magnitude and location of the temperature jump are observed, similar to previous results for the bulk. However, due to its depressed T_g at low cooling rates, no aging is observed for the ultrathin film under several conditions (T_a = 115.5 °C after q = 100 K/s and T_a 105.5 °C after q = 3 K/s) where aging is observed for the bulk – this is unambiguous evidence of the T_g depression in the ultrathin film sample. The apparent activation energy along the glass line is the same within experimental error for the ultrathin film and bulk, but the aging rate is slightly enhanced

for the 20 nm ultrathin film between 50 and 100 °C, in contrast to results for low fictive temperature glasses in the literature. The aging rate is shown to depend on two competing factors, namely the driving force or jump size ($T_f' - T_a$, or the distance from T_g) and the mobility or absolute aging temperature.

Acknowledgment

The authors gratefully acknowledge funding from NSF DMR 1006972.

References

1. McKenna, G. B. In Booth, C., Price, C., Eds.; *Comprehensive Polymer Science Polymer Properties*; Pergamon Press: Oxford, **1989**; Vol. 2. pp. 311-362.
2. McKenna, G. B.; Simon, S. L. In Cheng, S. Z. D., Ed.; *Handbook of Thermal Analysis and Calorimetry*; Elsevier Science: Amsterdam, **2002**; Vol. 3. pp. 49-109
3. Kovacs, A. J. *Adv. Polym. Sci.* **1963**, 3, 394.
4. Hutchinson J. M. *Prog. Polym. Sci.* **1995**, 20, 703.
5. Hodge, I. M. *J. Non-Cryst. Solids* **1994**, 169, 211.
6. McKenna, G. B.; Simon, S. L. *Macromolecules* **2017**, 50, 6333.
7. Priestley R. D.; Ellison C. J.; Broadbelt L. J.; Torkelson J. M., *Science* **2005**, 309, 456.
8. Koh Y. P.; Simon S. L. *J. Polym. Sci. Part B Polym. Phys*. **200**8, 46, 2741.
9. Guo Y.; Zhang C.; Lai C.; Priestley R. D.; Acunzi M. D.; Fytas G., *ACS Nano* **2011**, 5, 5365.
10. Pye J. E.; Rohald K. A.; Baker E. A.; Roth C. B., *Macromolecules* **2010**, 43, 8296.
11. Frieberg B.; Glynos E.; Green P. F., *Phys. Rev. Lett*. **2012**, 268304.
12. Guo Y.; Priestley R. D. In Napolitano S., Ed; *Non-equilibrium Phenomena In Confined Soft Matter, Soft and Biological Matter*; Springer: Switzerland**, 2015**; pp. 47-88.
13. Cangialosi D.; Alegria A.; Colmenero J., *Prog. Polym. Sci*. **2016**, 54-55, 128.
14. Koh Y. P.; Simon S. L., *J. Chem. Phys***. 2017**, 146, 203329.
15. Simon S. L.; Koh Y. P. In *Fast Scanning Calorimetry*; Springer: Switzerland, **2016**; 433-459.
16. Bian Y.; Pejanovic S.; Kenny J.; Mijovic J., *Macromolecules* **2007**, 40, 6239.
17. Boucher V. M.; Cangialosi D.; Alegria A.; Colmenero J.; Gonzalez-Irun, J.; Liz-Marzan L. M., *Soft Matter* **2010**, 6, 3306.
18. Koh Y. P.; Grassia L.; Simon S. L., *Thermochim. Acta* **2015**, 603, 135.

19. Koh Y. P; Gao S. Y.; Simon S. L., *Polymer* **2016**, 96, 182.

20. Lopez E.; Simon S. L., *Macromolecules* **2016**, 49, 2365.

21. Gao S. Y.; Koh Y. P; Simon S. L., *Macromolecules* **2013**, 46, 562.

22. Tool A. Q. *J. Am. Ceram. Soc.* **1946**, 29, 240-253.

23. Badrinarayanan P.; Zheng W.; Li Q. X. Simon S. L. *J. Non-Cryst. Solids* **2007**, 353, 2603-2612.

24. Keddie J. L.; Jones R. A. L.; Cory R. A., Faraday Discuss **1994**, 98, 219.

25. Roth C. B.; Dutcher J. R., J. Electroanal. Chem. **2005**, 584, 13.

26. Ellison C. J.; Torkelson J. M., Nature Mater. **2003**, 2, 695.

27. Schönhals A.; Goering H.; Schick C.; Frick B.; Zorn R., *J. Non-Cryst. Solids* **2005**, 351, 2668.

28. Fakhraai Z.; Forrest J. A., *Phys. Rev. Lett.* **2005**, 95, 025701.

29. Williams, M. L.; Landel, R. F.; Ferry, J. D. *J. Am. Chem. Soc.* **1955**, 77, 3701.

30. Kolla S.; Simon S. L., *Polymer* **2005**, 46, 733.

Figure captions

Figure 1. Flash DSC heating scans as a function of the cooling rate (q) ranging from 0.1 to 1000 K/s for the 20 nm thick polystyrene ultrathin film (blue) and the 1.1 μm thick polystyrene thin film (red). Inset shows the same data on a temperature scale from 50 to 150 °C.

Figure 2. (a) Glass transition temperature as a function of the logarithm of the cooling rate (q) for the 20 nm thick polystyrene ultrathin film (blue) and the 1.1 μm thick polystyrene thin film (red). (b) The equilibrium relaxation time as a function of T_f' for the same samples. The solid lines represent the WLF fits.

Figure 3. Representative Flash DSC heating scans as a function of aging time at T_a = 100.5 °C after cooling at 1000 K/s for the 20 nm thick polystyrene ultrathin film (blue) and the 1.1 μm thick polystyrene thin film (red).

Figure 4. Evolution of fictive temperature during isothermal aging at (a) T_a = 100.5, 105.5, 110.5, 115.5, and 120.5 °C and (b) at T_a = 50.5, 60.5, 70.5, 80.5, and 90.5 °C, both after cooling at 1000 K/s for the 20 nm thick polystyrene ultrathin film. (c) The reduced curves obtained from temperature-aging time superposition with 90.5 °C as the reference curve. Lines are a guide to the eye only.

Figure 5. Arrhenius plot of the shift factor a_T for the 20 nm thick polystyrene ultrathin film (blue) and the 1.1 μm thick polystyrene thin film (red). The slopes represent the normalized apparent activation energy along the glass line. The empty symbols are for T_a = 115.5 °C and are not included in the fit.

Figure 6. Aging rate (R) as a function of aging temperature (T_a) for the 20 nm thick polystyrene ultrathin film (blue) and the 1.1 μm thick polystyrene thin film (red).

Figure 7. Evolution of fictive temperature during isothermal aging at T_a = 100.5, 105.5, 110.5, 115.5, and 120.5 °C after cooling at (a) 100 K/s, (b) 3 K/s, and (c) 0.3 K/s for the 20 nm thick polystyrene ultrathin film. Lines are a guide to the eye only.

Figure 8. The cooling rate dependence of the aging rate (R) at T_a = 100.5, 105.5, 110.5, 115.5, and 120.5 °C for the 20 nm thick polystyrene ultrathin film. The inset shows the dependence of aging rate on initial fictive temperature. Lines are a guide to the eye only.

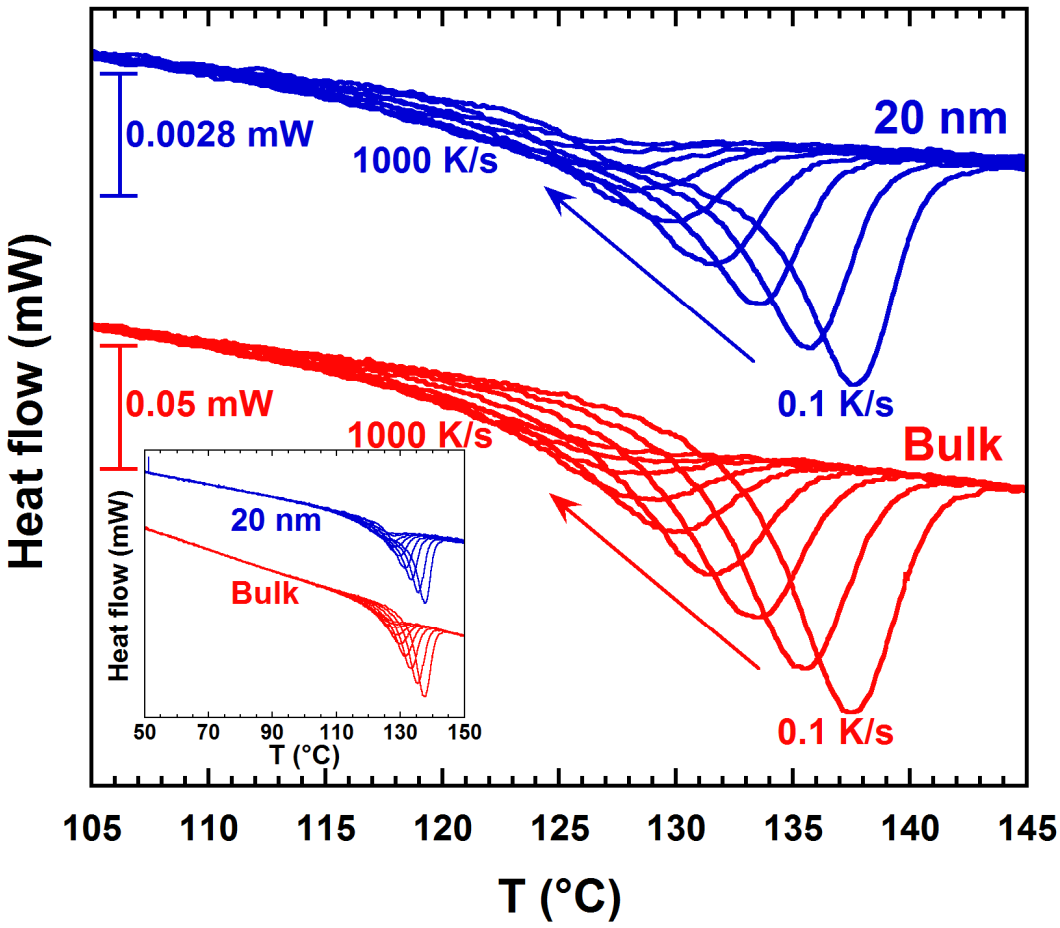

Figure 1. Flash DSC heating scans as a function of the cooling rate (q) ranging from 0.1 to 1000 K/s for the 20 nm thick polystyrene ultrathin film (blue) and the 1.1 μm thick polystyrene thin film (red). Inset shows the same data on a temperature scale from 50 to 150 °C.

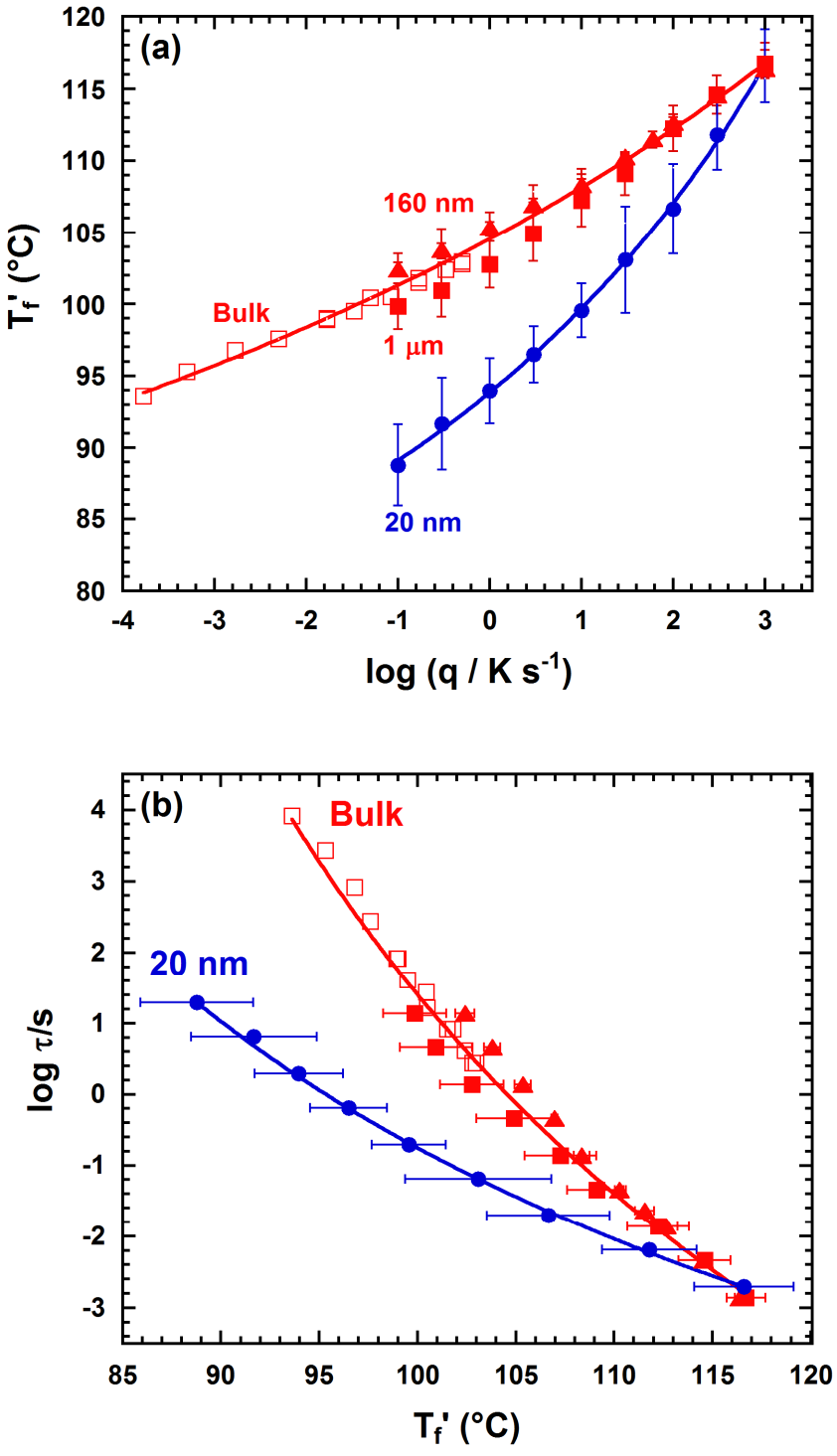

Figure 2. (a) Glass transition temperature as a function of the logarithm of the cooling rate (q) for the 20 nm thick polystyrene ultrathin film (blue) and the 1.1 µm thick polystyrene thin film (red). (b) The equilibrium relaxation time as a function of T_f' for the same samples. The solid lines represent the WLF fits.

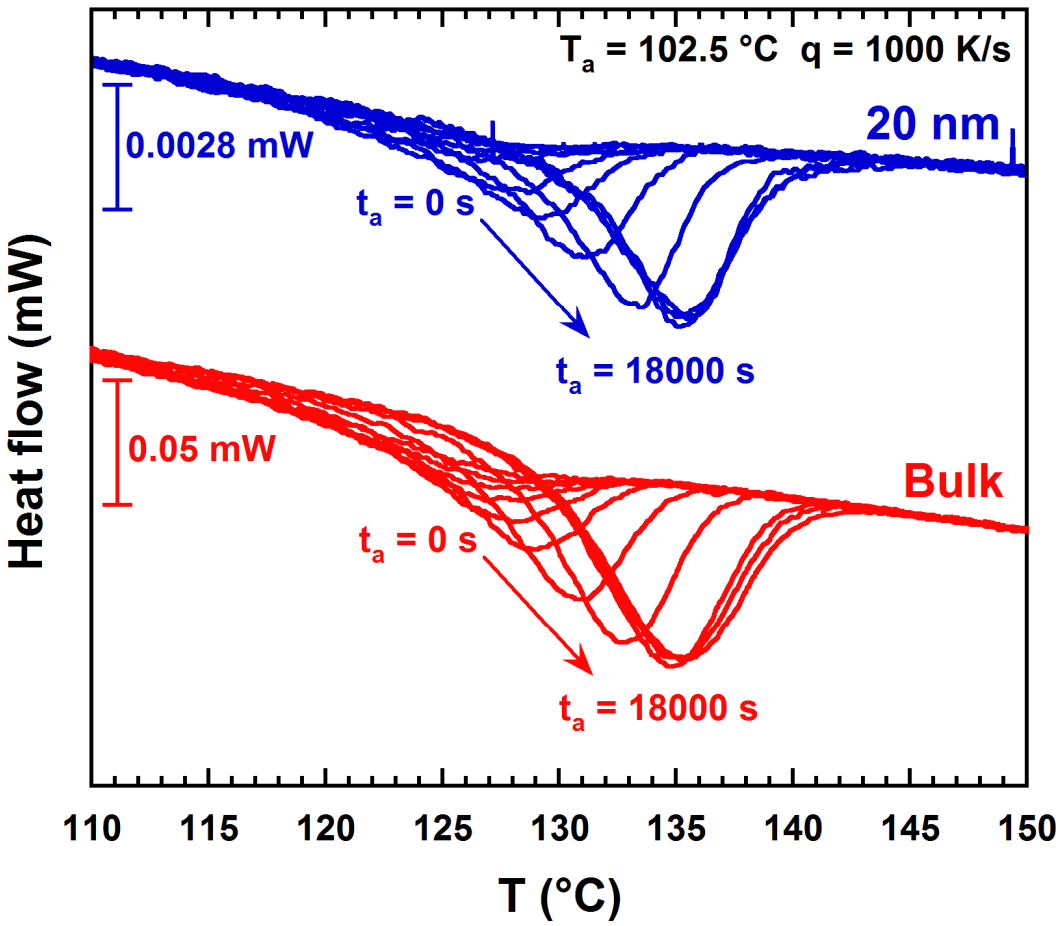

Figure 3. Representative Flash DSC heating scans as a function of aging time at T_a = 100.5 °C after cooling at 1000 K/s for the 20 nm thick polystyrene ultrathin film (blue) and the 1.1 μm thick polystyrene thin film (red).

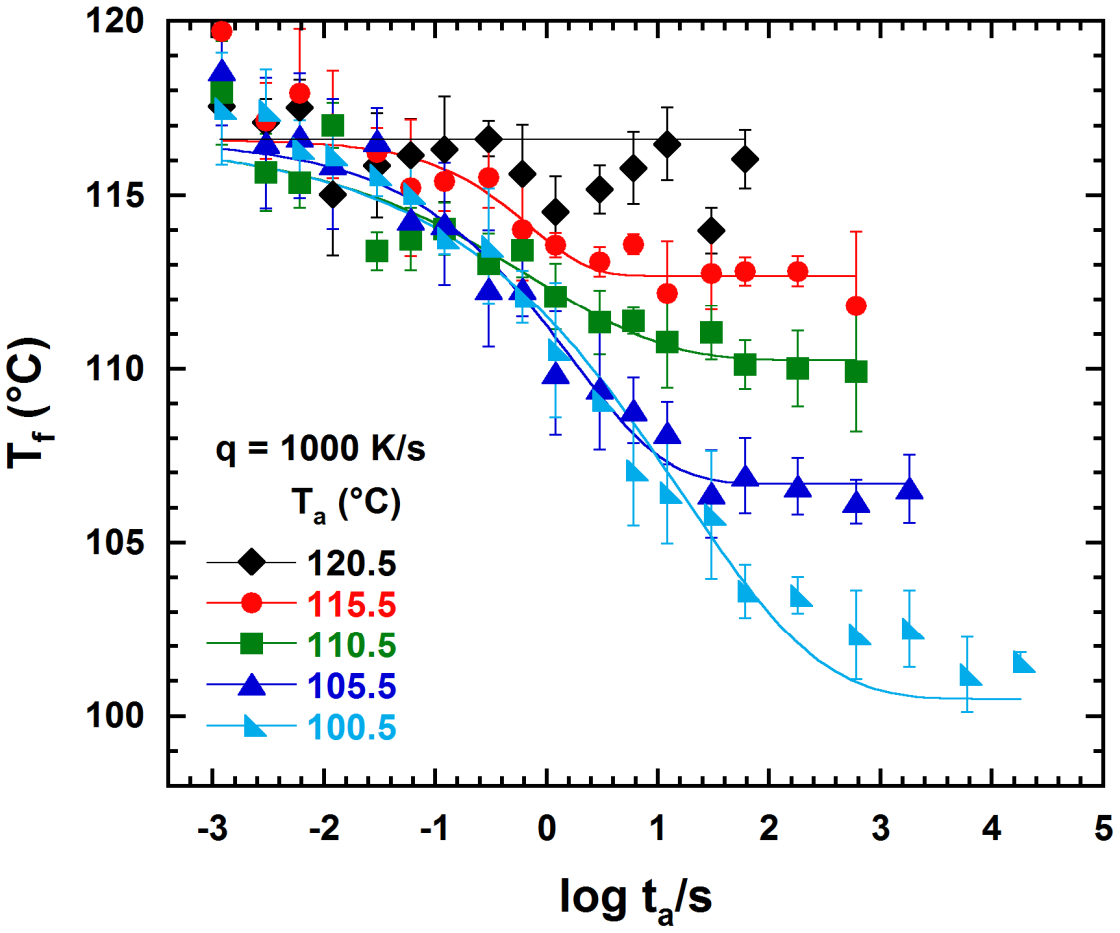

Figure 4a. Evolution of fictive temperature during isothermal aging at T_a = 100.5, 105.5, 110.5, 115.5, and 120.5 after cooling at 1000 K/s for the 20 nm thick polystyrene ultrathin film. Lines are a guide to the eye only.

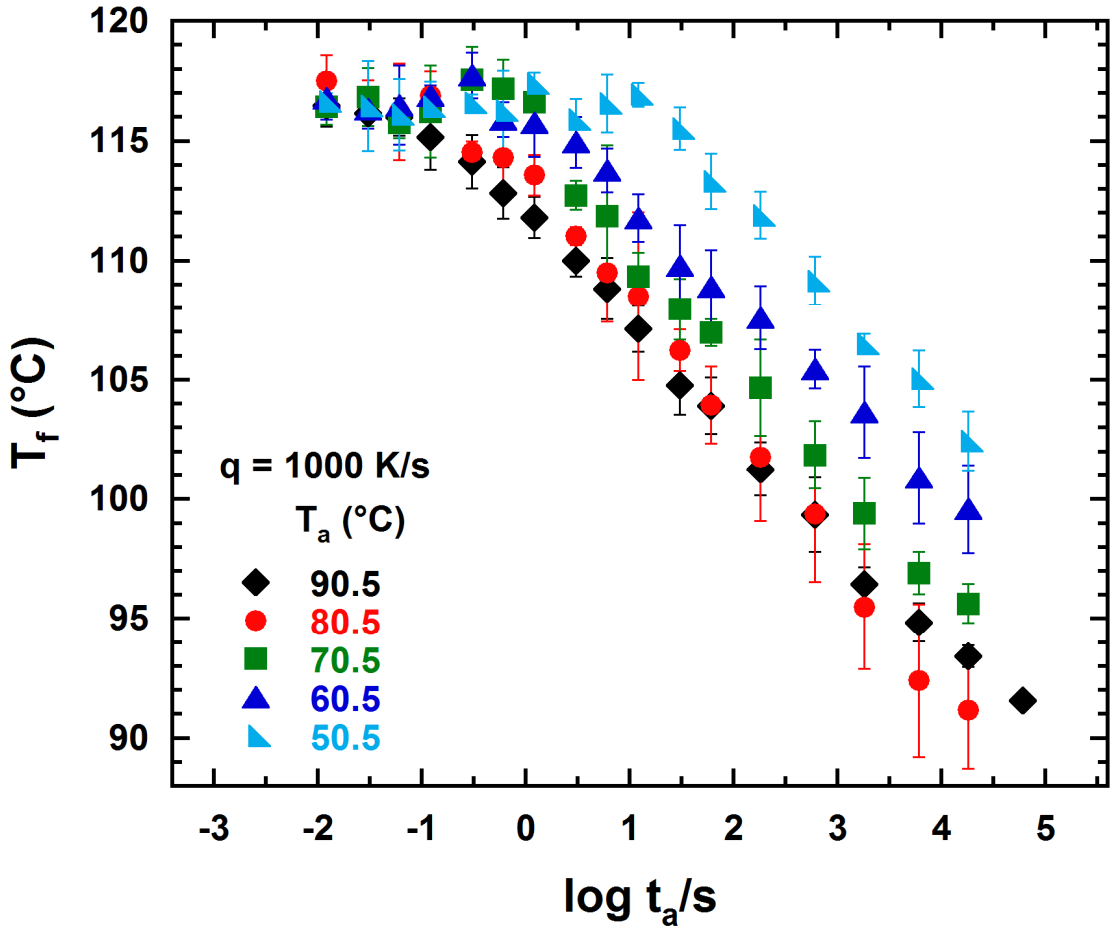

Figure 4b. Evolution of fictive temperature during isothermal aging at T_a = 50.5, 60.5, 70.5, 80.5, and 90.5 °C after cooling at 1000 K/s for the 20 nm thick polystyrene ultrathin film.

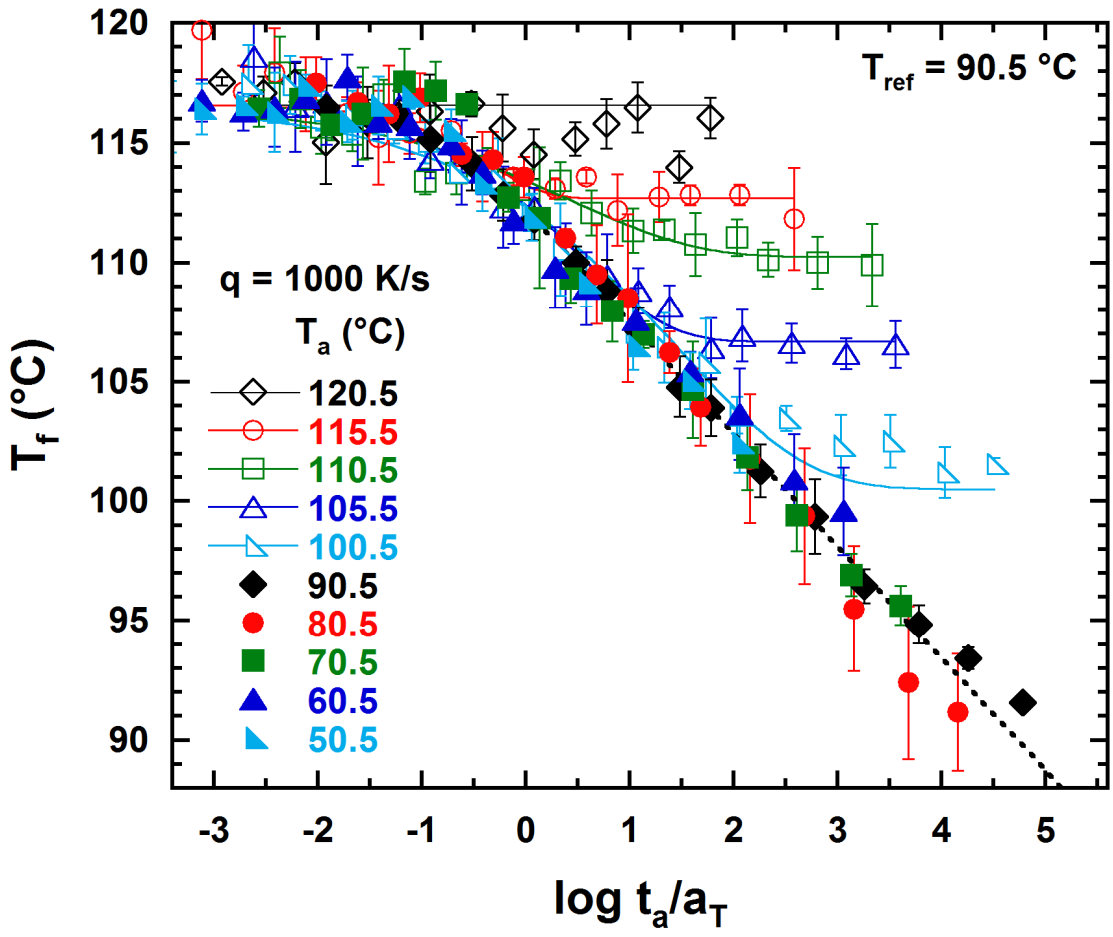

Figure 4c. The reduced curves obtained from temperature-aging time superposition with 90.5 °C as the reference curve. Lines are a guide to the eye only.

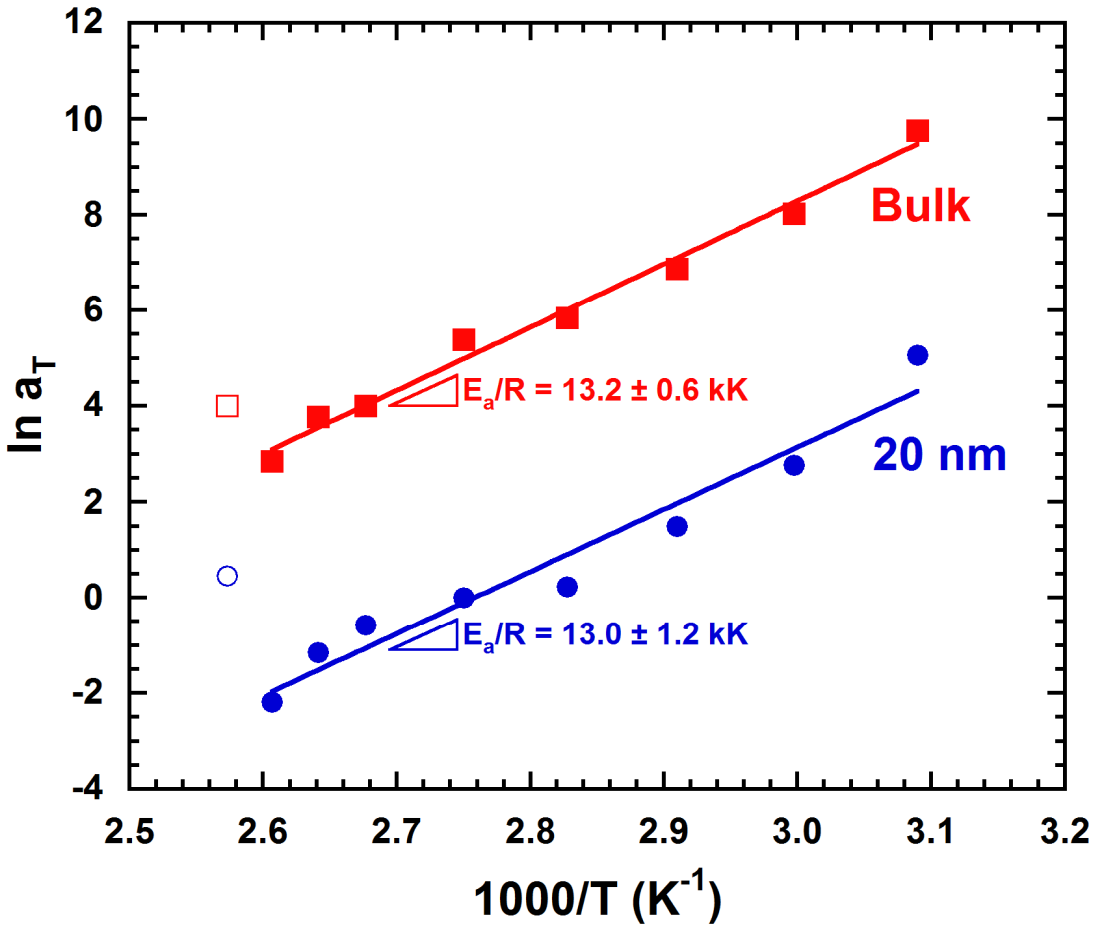

Figure 5. Arrhenius plot of the shift factor a_T for the 20 nm thick polystyrene ultrathin film (blue) and the 1.1 μm thick polystyrene thin film (red). The slopes represent the normalized apparent activation energy along the glass line. The empty symbols are for T_a = 115.5 °C and are not included in the fit.

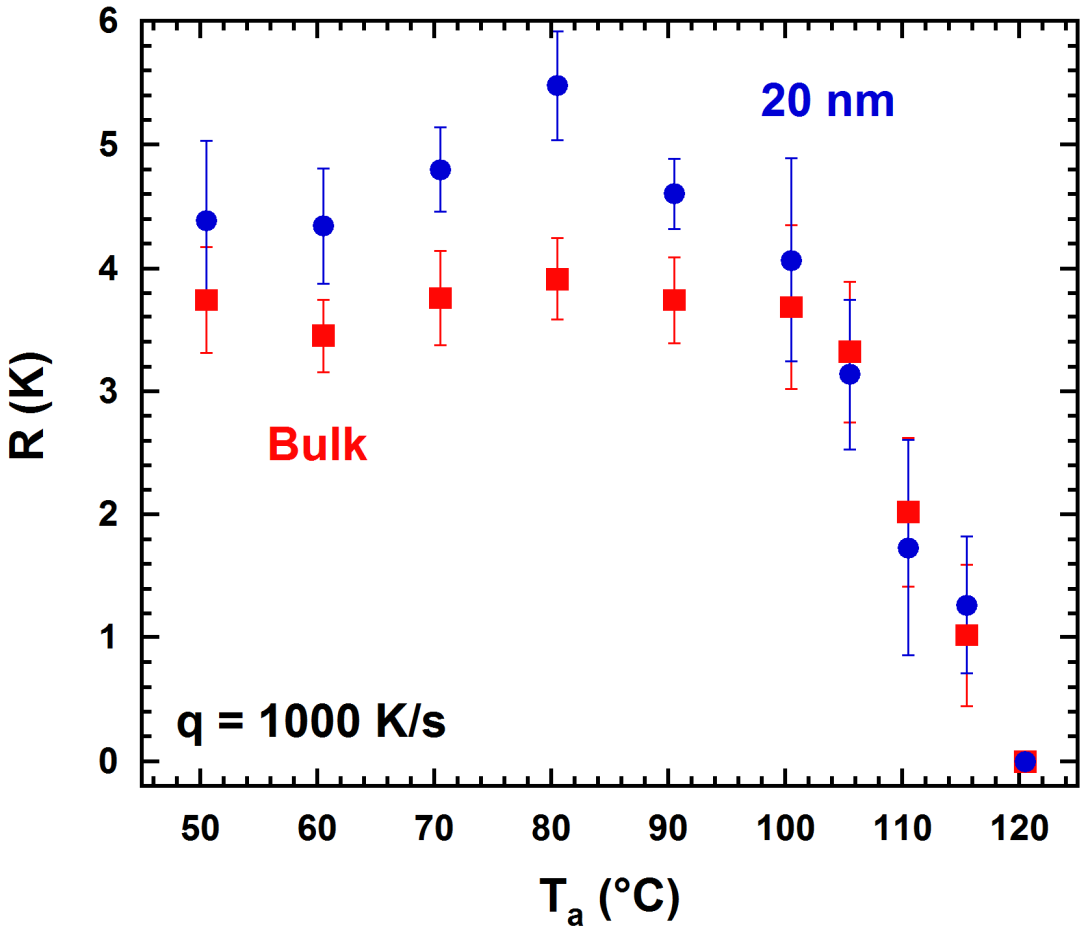

Figure 6. Aging rate (R) as a function of aging temperature (T_a) for the 20 nm thick polystyrene ultrathin film (blue) and the 1.1 μm thick polystyrene thin film (red).

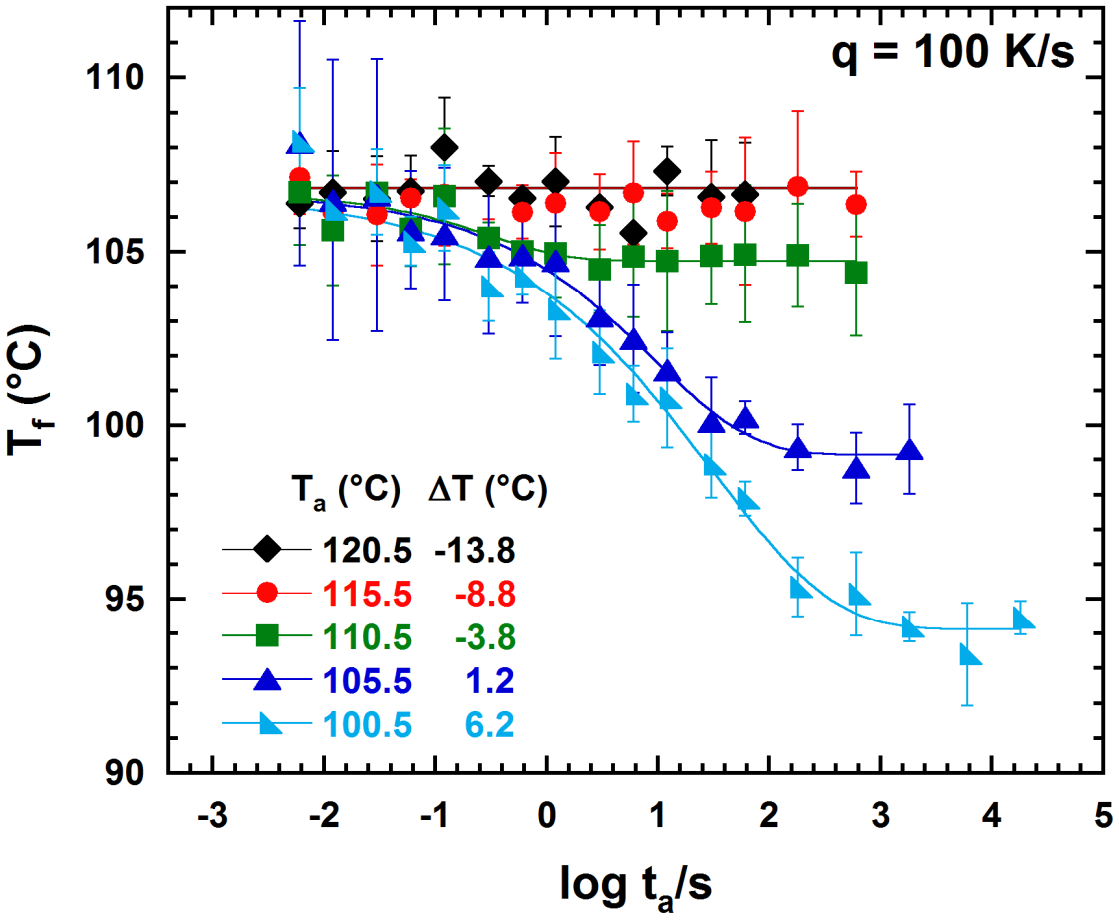

Figure 7a. Evolution of fictive temperature during isothermal aging at T_a = 100.5, 105.5, 110.5, 115.5, and 120.5 °C after cooling at 100 K/s for the 20 nm thick polystyrene ultrathin film. Lines are a guide to the eye only.

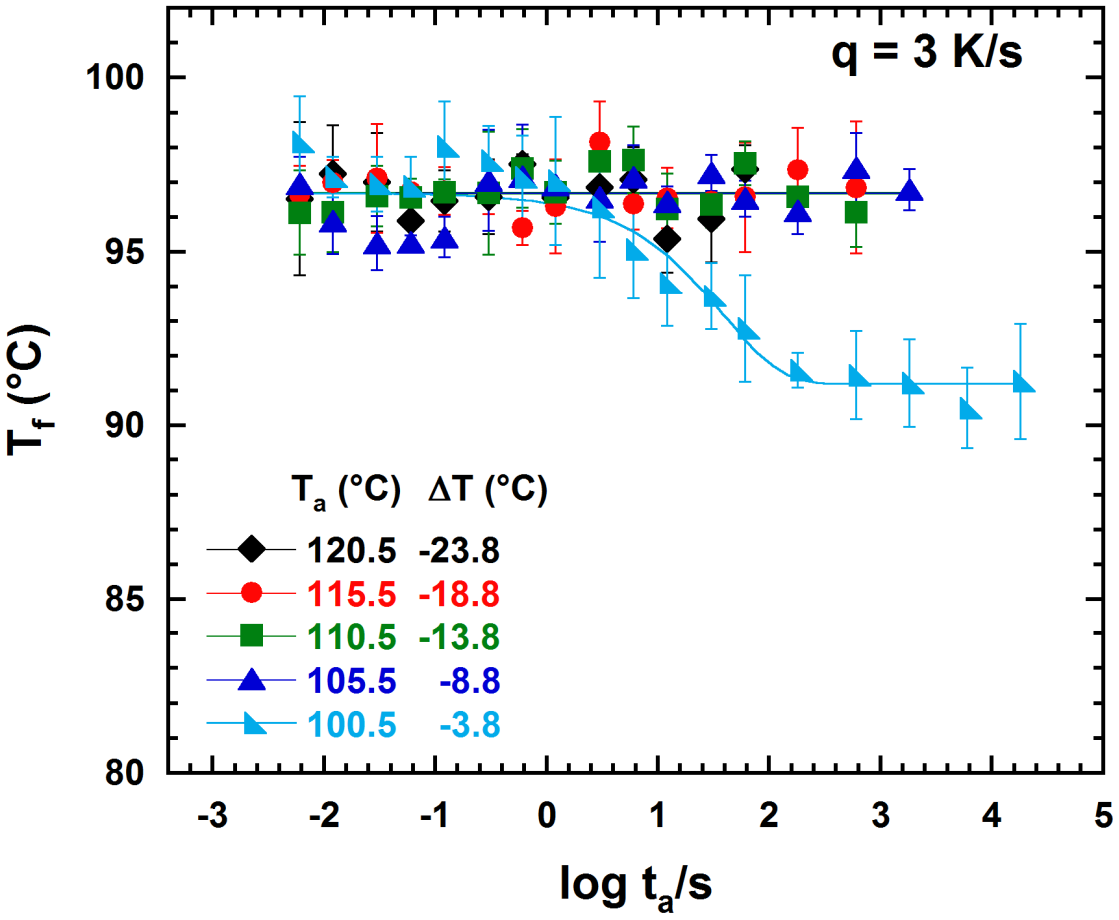

Figure 7b. Evolution of fictive temperature during isothermal aging at T_a = 100.5, 105.5, 110.5, 115.5, and 120.5 °C after cooling at 3 K/s for the 20 nm thick polystyrene ultrathin film. Lines are a guide to the eye only.

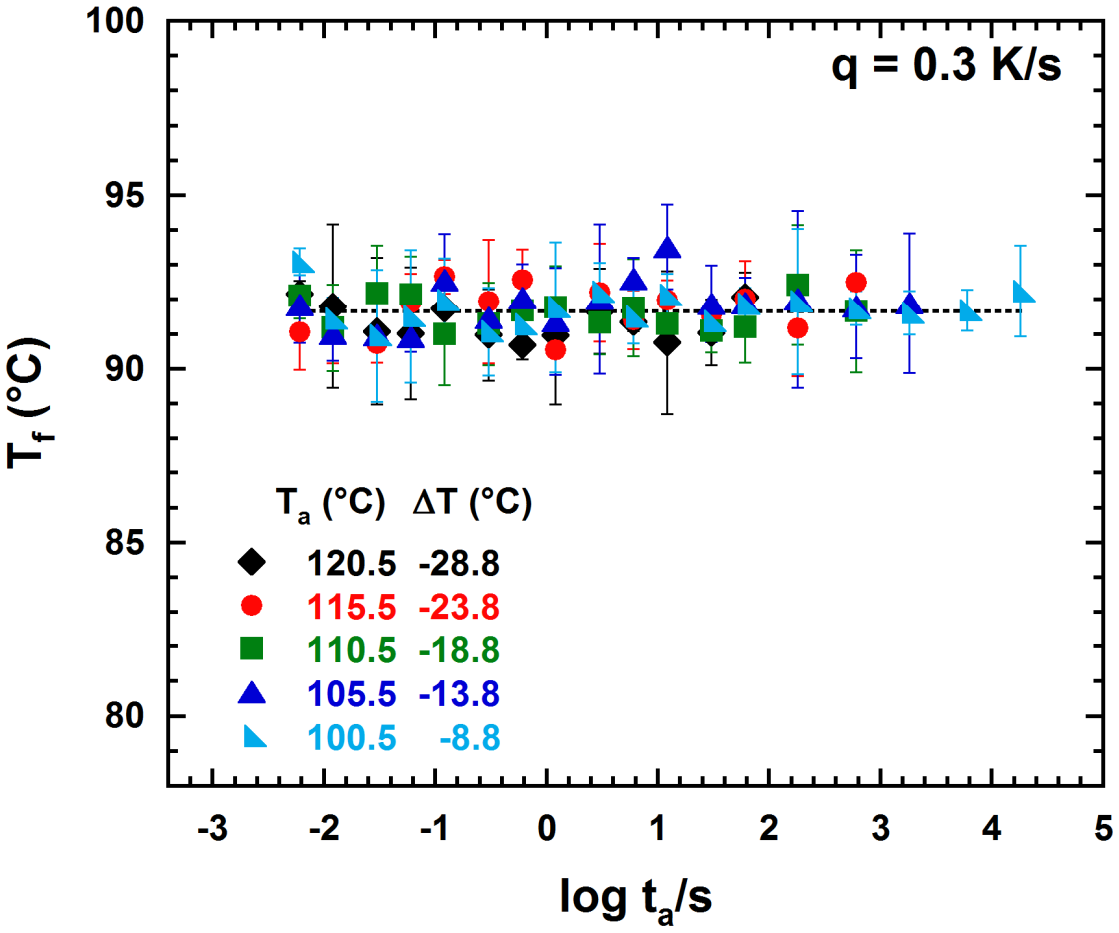

Figure 7c. Evolution of fictive temperature during isothermal aging at T_a = 100.5, 105.5, 110.5, 115.5, and 120.5 °C after cooling at 0.3 K/s for the 20 nm thick polystyrene ultrathin film. Lines are a guide to the eye only.

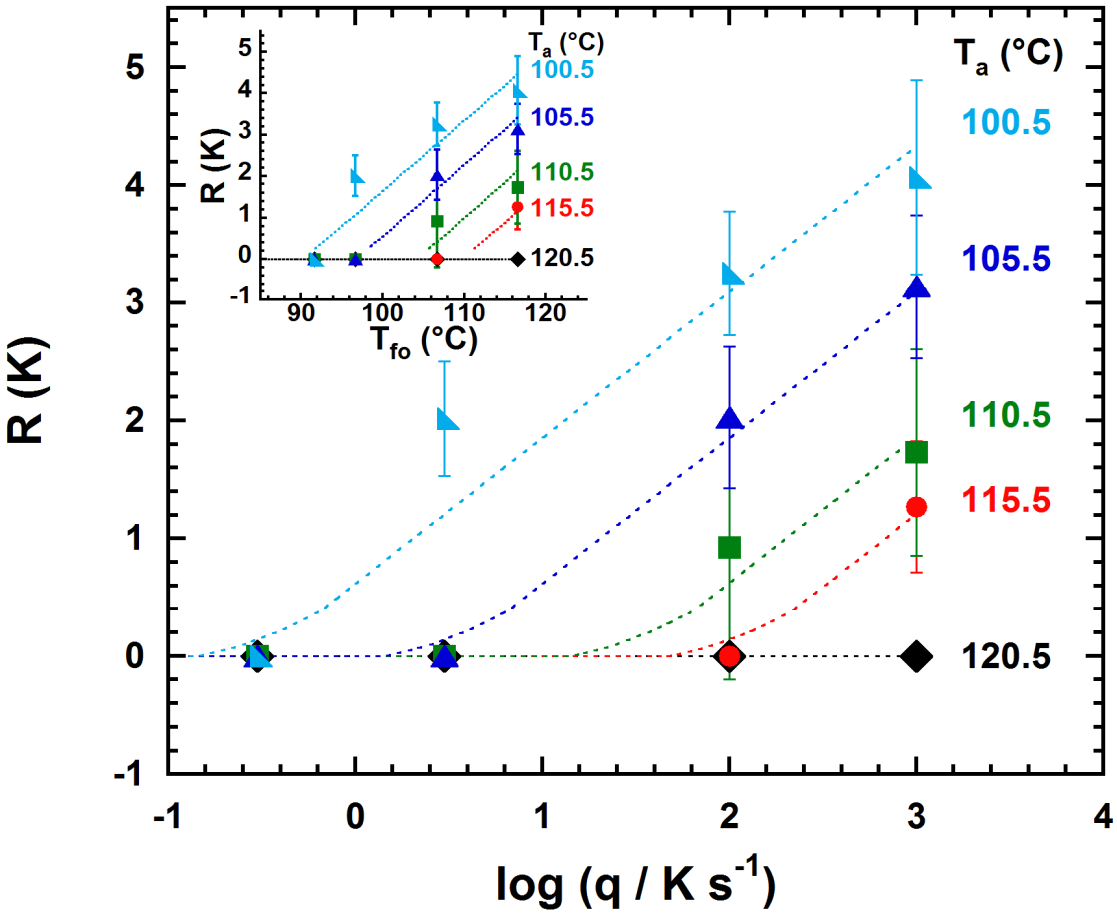

Figure 8. The cooling rate dependence of the aging rate (R) at T_a = 100.5, 105.5, 110.5, 115.5, and 120.5 °C for the 20 nm thick polystyrene ultrathin film. The inset shows the dependence of aging rate on initial fictive temperature. Lines are a guide to the eye only.

Enthalpy Recovery of Ultrathin Polystyrene Film Using Flash DSC

Yung P. Koh and Sindee L. Simon

Department of Chemical Engineering, Texas Tech University, Lubbock, TX 79409-3121, USA

HIGHLIGHTS

Enthalpy recovery for a 20 nm thick polystyrene is studied using Flash DSC.

Compared to bulk, the thin film has a broader and depressed T_g.

The thin film shows no aging for several conditions where aging occurs for the bulk.

The aging rate depends on two competing factors: jump size and aging temperature.

The aging rate is faster for the thin film at temperatures between 60 and 100 °C.